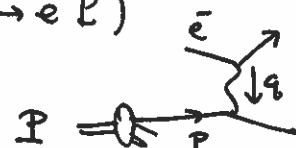


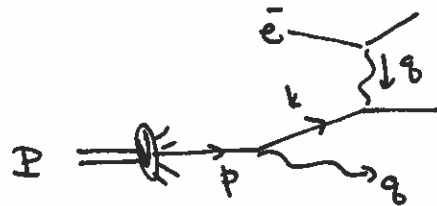
Parton Distribution Functions

In the previous lecture, we saw how radiation of almost collinear partons forms the shapes of jets and organizes the final states in e^+e^- annihilation. You might expect that, in processes with initial hadrons that we describe with the parton model, there should be a similar effect on initial state partons.

We can analyze this for deep inelastic scattering. Our formula for the cross section was

$$\sigma = \int dx \sum_f f_f(x) \sigma(e^- q(xP) \rightarrow e^- P)$$


Now include radiation of a collinear gluon from the initial quark.



Again, we can factorize this diagram on a quark propagator that is nearly on shell. The kinematics is slightly different from that in final state radiation. Now it is the initial quark p that is on shell and the quark k after radiation that is off shell. The momentum q of the emitted gluon is on shell. Then the three momenta are

$$p = (E, 0, 0, E)$$

$$q = \left((1-z)E, k_T, 0, (1-z)E - \frac{k_T^2}{2(1-z)E} \right)$$

$$k = \left(zE, -k_T, 0, zE + \frac{k_T^2}{2(1-z)E} \right)$$

and so

$$k^2 = -k_T^2 - \frac{2k_T^2}{(1-z)} = -\frac{k_T^2}{(1-z)}$$

Note that, for convenience here, I have exchanged $z \leftrightarrow (1-z)$. Since, aside from this, the vectors above differ from the ones we used in the previous lecture only in order k_T^2 , our calculation of the gluon emission matrix element in the previous lecture can be used here without change.

Factorizing the matrix element for $e^-q \rightarrow e^-qg$ on the propagator of k , we find

$$\sigma(\bar{e}q \rightarrow \bar{e}qg) = \frac{1}{2xs} \int \frac{d^3q}{(2\pi)^3 2q} \int d\Pi_2 |\mathcal{M}(q \rightarrow qg)|^2 \frac{(1-z)^2}{k_T^4} |\mathcal{M}(\bar{e}q(xz) \rightarrow \bar{e}q)|^2$$

where $d\Pi_2$ is the phase space integral over the final electron and quark. The gluon phase space can be rewritten as

$$\int \frac{d^3q}{(2\pi)^3 2q} = \int \frac{dk_T k_T 2\pi dz E}{16\pi^3 (1-z)E} = \int \frac{dk_T k_T dz}{8\pi^2 (1-z)}$$

Then the cross section for the e^-q scattering process becomes

$$\begin{aligned} \sigma(\bar{e}q(xz) \rightarrow \bar{e}qg) &= \frac{1}{2xs} \int \frac{dk_T k_T dz}{8\pi^2 (1-z)} \left[\frac{4}{3} g^2 \frac{(1+z^2) 2k_T^2}{(1-z)^2 z} \right] \frac{(1-z)^2}{k_T^4} \\ &\quad \cdot \int d\Pi_2 |\mathcal{M}(\bar{e}q(xz) \rightarrow \bar{e}q)|^2 \\ &= \int \frac{dk_T}{k_T} \frac{\alpha_s}{\pi} \int dz \frac{4}{3} \frac{1+z^2}{(1-z)} \frac{1}{2xs} \int d\Pi_2 |\mathcal{M}(\bar{e}q(xzs) \rightarrow \bar{e}q)|^2 \end{aligned}$$

Integrating this over the parton distribution for the quark in the proton, we find

$$\sigma(\bar{e}p \rightarrow \bar{e}gg) = \int dx \sum_f f_f(x) \int \frac{dk_T}{k_T} \frac{\alpha_s}{\pi} \int dz P_{g \rightarrow g}(z) \cdot \sigma(\bar{e}q(xz) \rightarrow \bar{e}g)$$

In principle, the initial parton could also be a gluon that splits to a quark or antiquark. For the full contribution to deep inelastic scattering with radiation, we must sum over all possibilities.

Again, we find a logarithmically infrared divergent cross section. I will control this divergence just as I did for the fragmentation function, by summing up the contributions of multiplet emissions using a differential equation.

The collinear divergence in this equation is building up structure in the parton distribution function. Thus, we should sum it as an evolution of the parton distributions. In the equation above, the quark that enters the e^-q scattering process comes from a quark radiating a gluon, but there is another contribution in which the struck quark comes from a gluon splitting. Thus, we should include all possible partons in the proton as initial partons from which this quark might be obtained. Then we can follow the logic of the previous lecture and derive the Altarelli-Parisi equation

$$\frac{d}{d \log Q} f_P(x, Q) = \frac{\alpha_s(Q)}{\pi} \int \frac{dz}{z} \sum_{P'} f_{P'}\left(\frac{x}{z}, Q\right) P_{P' \rightarrow P}(z)$$

where now

$$dz f_P(x, Q)$$

is the probability of finding the parton P at the fraction x of the proton's momentum when emissions with $k_T < Q$ are accounted. Since the transverse momentum of the emission will not be greater than the momentum imparted to the proton by the electron, this function also represents the parton distribution observed in a deep inelastic scattering process with momentum transfer Q^2 from the electron.

The Altarelli-Parisi equation implies that the parton distributions are not static with Q^2 as I suggested in last Friday's lecture. Rather, they evolve with the scale of the hard scattering momentum. This evolution takes place on a log scale in Q , so it is difficult to see unless an experiment spans a very broad range in Q . The physics of

this evolution is that quarks and gluons resolve their structure at smaller distances or larger Q by splitting into collinear pairs of quarks and gluons. This has two important effects. First, the partons found at high x at low Q move to lower values of x at high Q due to parton radiation. Second, splitting produces new quarks, antiquarks, and gluons at very small x whose number increases as Q increases. Figs p. 2 shows a solution to the Altarelli-Parisi equations for the u quark distribution in the proton at $Q = 2, 20,$ and 200 GeV. You can see both of these effects operating in this plot.

Some experimental data on the evolution of parton distributions are shown in the next two figures. Figs p. 3 shows most of the world's data on

$$F_2(x) = \sum_f Q_f^2 \times (f_f(x) + f_{\bar{f}}(x))$$

obtained from deep inelastic scattering experiments from SLAC to HERA. The data is plotted as a function of Q^2 over many decades, in bins in x . You can see the decrease of $F_2(x, Q^2)$ in the high x bins and the increase in F_2 at low x . The blue lines are a solution to the Altarelli-Parisi equations. One of the most important effects of parton evolution is the growth of the gluon distribution at small x , due to the small- x behavior of the $g \rightarrow gg$ splitting function

$$P_{g \rightarrow g}(z) \sim \frac{6}{z} \quad z \rightarrow 0$$

The gluon distribution grows rapidly, and then becomes visible in F_2 through gluon splitting to a quark-antiquark pair. Figs p. 4 shows $F_2(x)$ at very small x and two values of Q^2 , as measured at HERA, compared to a QCD model. The presence of large numbers of quarks and antiquarks signals the presence of large numbers of gluons, and so the evolution of these distributions can be used to determine the gluon parton distribution in the proton.

To determine the separate parton distributions for all parton species, we need to assemble results from a number of experiments. Electron deep inelastic scattering measures only the particular combination F_2 written above. At SLAC, experimenters also measured deep inelastic scattering on a deuterium target. By isospin symmetry, the up quark distribution in the neutron is equal to the down quark distribution in the proton, and the distribution in the deuteron is the sum of these two. So this process accesses a different linear combination of the u and d quark distributions. Another method is to do deep inelastic scattering by weak interactions using a neutrino beam.

Neutrino deep inelastic scattering has many beautiful features that I hope you will learn through this week's problem set. As a preview, Figs p. 5 shows the dependence on y of neutrino deep inelastic scattering cross sections at various values of x . Figs p. 6 shows the Q^2 -dependence of $x(f_u(x) + f_d(x))$ extracted from neutrino experiments. Neutrinos can access higher values of x , and so you see a steeper falloff with Q^2 in the highest x bins. A solution to the Altarelli-Parisi equations is shown as a set of dotted lines.

As we will see in a moment, hadron-hadron scattering processes can also contribute to the measurement of parton distribution functions. Figs p. 7 shows data from the E866 experiment at Fermilab, which studied $\mu^+\mu^-$ production in pp and pd collisions in a fixed-target setting. High energy μ pairs are produced by annihilation of high-energy quarks in the proton beam with antiquarks in the target. If the \bar{u} and \bar{d} antiquark distributions in the proton were equal, the p and d targets would show such events precisely in the ratio 2:1. Instead, more annihilations are seen from the d target, demonstrating that there are more \bar{d} 's than \bar{u} 's in the proton.

By fitting all of this data to a common solution to the Altarelli-Parisi equation, we can arrive at a complete picture of the parton structure of the proton. Figs p. 8 shows the result of such an analysis by the Durham group, with the results evaluated at $Q = 10$ GeV. The contribution of the basic u and d quarks dominates at large x . Below $x = 0.1$, however, the gluon distribution takes off. When we boost protons to high energy, these gluons acquire high energy and gives very high rates for hard parton-parton collisions.

There should be c and b quarks in the proton, at least as the result of gluon splitting. The gluon can split to these heavy quarks just as easily as it splits to light quarks in the regime $Q > 2m$ where the mass of the heavy quarks can be ignored. A reasonable way to estimate the c and b content of the proton is to take the c and b parton distributions to be zero at low Q and then generate c and b by integrating the Altarelli-Parisi equation. Figs p. 8 compares c and b parton distributions constructed in that way with data on c and b production in electron-proton scattering at HERA.

If the parton model gives a good description of electron-proton scattering, it ought also to be useful in describing hard-scattering reactions in proton-proton scattering. The proton-proton cross section measured at high energy is very large, about 70 mb at 2 TeV in the center of mass. However, most of that cross section consists of processes with low momentum transfer that softly break up the bags of quarks and gluons. We are more interested in the hard-scattering processes that throw quarks, gluons, and leptons out to large momenta. In QCD, these reactions are mediated by the weak coupling part of the theory and can be estimated using QCD perturbation theory.

To compute cross sections, we use the parton model to describe both of the colliding hadrons. That is,

$$\sigma(pp \rightarrow \mathbb{X}) = \int dx_1 \sum_{P_1} f_{P_1}(x_1) \int dx_2 \sum_{P_2} f_{P_2}(x_2) \sigma(P_1(x_1) P_2(x_2) \rightarrow \mathbb{X})$$

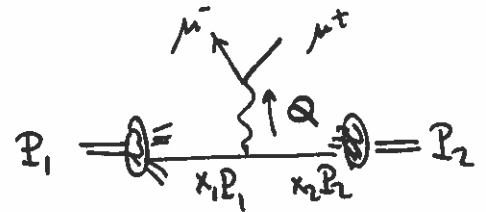
The simplest application of this formula is to the *Drell-Yan process*, $pp \rightarrow \mu^+ \mu^-$. At the parton level, the basic process is $q\bar{q}$ annihilation to a lepton pair, the reverse of the process $e^+e^- \rightarrow q\bar{q}$. The cross section for this process is

$$\sigma(q_f \bar{q}_f \rightarrow \mu^+ \mu^-) = \frac{4\pi\alpha^2}{3\hat{s}} \cdot Q_f^2 \cdot \frac{1}{3}$$

where \hat{s} is the squared center of mass energy of the parton-parton collision. Instead of the factor 3 in the earlier case, a factor $\frac{1}{3}$ appears here. This is because the initial state quarks have random colors, but the quark and antiquark that annihilate must have the same color. A more formal way to see this is that the cross section for annihilation of a quark of color i with an antiquark of color j must have a δ_{ij} . Then the average of this cross section over initial colors gives

$$\frac{1}{3} \cdot \frac{1}{3} \cdot \sum_{ij} \delta_{ij} = \frac{1}{3}$$

The Drell-Yan cross section is then



$$\sigma(pp \rightarrow \mu^+ \mu^-) = \sum_f \int dx_1 dx_2 \left[f_f(x_1) f_{\bar{f}}(x_2) + f_{\bar{f}}(x_1) f_f(x_2) \right] \frac{Q_f^2}{3} \frac{4\pi\alpha^2}{3\hat{s}}$$

One proton gives the quark, the other the antiquark, and we must sum over both possibilities.

Since we observe the final muon pair, we can learn something about the momentum fractions of the quark and antiquark that annihilated. The value of \hat{s} , from the initial state, is

$$\hat{s} = (p_1 + p_2)^2 = (x_1 \hat{P}_1 + x_2 \hat{P}_2)^2 = 2x_1 x_2 \hat{P}_1 \cdot \hat{P}_2 = x_1 x_2 S$$

This is also the value of the observed mass of the dimuon system

$$m^2(\mu^+\mu^-) = Q^2 = x_1 x_2 S$$

so this is one constraint on the values x_1, x_2 . An orthogonal constraint comes from the boost of the dimuon system. In the parton model, the muon pair has a total momentum that is approximately collinear with the beam direction. The value of the momentum is

$$\hat{Q}^\mu = x_1 \hat{P}_1^\mu + x_2 \hat{P}_2^\mu = ((x_1 + x_2)E, 0, 0, (x_1 - x_2)E)^\mu$$

A convenient way to parametrize this is as

$$\hat{Q}^\mu = (Q \cosh y, 0, 0, Q \sinh y)^\mu$$

The parameter y called the *rapidity*. Lorentz boosts are simple translations of rapidity. Comparing these expressions,

$$\tanh y = \frac{x_1 - x_2}{x_1 + x_2} \quad \Leftrightarrow \quad y = \frac{1}{2} \log \frac{x_1}{x_2}$$

From the observed momenta of the muon pair, we can determine Q^2 and y and, from these, solve for x_1 and x_2

It is useful to change variables from (x_1, x_2) to (y, Q^2) . The Jacobian is

$$\frac{\partial(y, Q^2)}{\partial(x_1, x_2)} = \begin{vmatrix} \frac{1}{2x_1} & -\frac{1}{2x_2} \\ x_2 s & x_1 s \end{vmatrix} = s = \frac{Q^2}{x_1 x_2}$$

Then we can write the Drell-Yan cross section as

$$\frac{d\sigma}{dy dQ^2} (pp \rightarrow \mu^+ \mu^-) = \sum_f \left[x_1 f_f(x_1) x_2 \bar{f}_f(x_2) + x_1 \bar{f}_f(x_1) x_2 f_f(x_2) \right] \cdot \frac{Q^2}{3} \cdot \frac{4\pi\alpha^2}{3Q^4}$$

This formula can be used to determine parton distributions for quarks and especially, as we have seen above, for antiquarks. Figs p. 10 shows a comparison of the parton model prediction for the Drell-Yan cross section (including order α_s higher-order QCD corrections) with the data on dimuon pair production from the CDF experiment at the Fermilab Tevatron, a 2 TeV $p\bar{p}$ collider.

We can also apply the parton model to quark-quark, quark-gluon, and gluon-gluon hard scattering processes. These processes kick two partons out at large transverse momentum with respect to the beam direction and so lead to 2-jet final states. Figs p. 11 shows a 2-jet event recorded by CDF. Only the highest-momentum tracks are shown in blue; there are many more low-momentum tracks indicated by the black hits in the tracking chamber. The energy deposition in the electromagnetic and hadron calorimeters is also shown.

Figs p. 12 shows another view of this event. Here the event is shown on the plane of azimuthal versus polar angle. The polar angle is described by the variable η , called *pseudorapidity*. For a massless particle, we can parametrize the momentum vector as

$$\vec{p}^\mu = (p_T \cosh \eta, \vec{p}_T, p_T \sinh \eta)^\mu$$

where here η is the rapidity. Generally, we do not know the mass for each final particle in a hadron collider event. But most of these particles are pions or photons from π^0 decay, so it is customary to ignore their masses and use η as a measure of the rapidity. From the formula above, η is simply a function of $\cos \theta$.

$$\eta = \frac{1}{2} \log\left(\frac{1+\cos\theta}{1-\cos\theta}\right)$$

But, approximately, a longitudinal boost of the event corresponds simply to a shift in η . In the figure, the energy deposited in each cell of the calorimeter is shown as a tower at its (θ, ϕ) or (η, ϕ) position. The event display is called the 'lego plot'. It is very useful for recognizing the high transverse momentum components of a hadron collider event.

The parton model cross section for 2 jet production is

$$\sigma = \int dx_1 dx_2 \int d\omega_{\theta_*} \sum_{\beta_1 \beta_2 \beta_3 \beta_4} f_{\beta_1}(x_1) f_{\beta_2}(x_2) \cdot \frac{d\sigma}{d\omega_{\theta_*}}(\beta_1 \beta_2 \rightarrow \beta_3 \beta_4)$$

where the last factor is the spin-averaged, color-averaged parton-parton differential cross section in the parton-parton center of mass frame. The lowest order formulae for these differential cross sections can be readily computed in QCD:

$$\frac{d\sigma}{d\omega_{\theta_*}}(ud \rightarrow ud) = \frac{2}{9} \frac{\pi \alpha_s^2}{S} \left[\frac{\hat{u}^2 + \hat{s}^2}{\hat{t}^2} \right]$$

$$\frac{d\sigma}{d\omega_{\theta_*}}(uu \rightarrow uu) = \frac{2}{9} \frac{\pi \alpha_s^2}{S} \left[\frac{\hat{u}^2 + \hat{s}^2}{\hat{t}^2} + \frac{\hat{t}^2 + \hat{s}^2}{\hat{u}^2} - \frac{2}{3} \frac{\hat{s}^2}{\hat{u}\hat{t}} \right]$$

$$\frac{d\sigma}{d\omega_{\theta_*}}(u\bar{u} \rightarrow d\bar{d}) = \frac{2}{9} \frac{\pi \alpha_s^2}{S} \left(\frac{\hat{u}^2 + \hat{t}^2}{\hat{s}^2} \right)$$

$$\frac{d\sigma}{d\omega_{\theta_*}}(u\bar{u} \rightarrow u\bar{u}) = \frac{2}{9} \frac{\pi \alpha_s^2}{S} \left[\frac{\hat{u}^2 + \hat{t}^2}{\hat{s}^2} + \frac{\hat{u}^2 + \hat{s}^2}{\hat{t}^2} - \frac{2}{3} \frac{\hat{u}^2}{\hat{s}\hat{t}} \right]$$

$$\frac{d\sigma}{d\cos\theta_*} (u\bar{u} \rightarrow gg) = \frac{16}{27} \frac{\pi\alpha_s^2}{s} \left[\frac{\hat{u}}{\hat{t}} + \frac{\hat{t}}{\hat{u}} - \frac{9}{4} \frac{\hat{u}^2 + \hat{t}^2}{\hat{s}^2} \right]$$

$$\frac{d\sigma}{d\cos\theta_*} (gg \rightarrow u\bar{u}) = \frac{1}{12} \frac{\pi\alpha_s^2}{s} \left[\frac{\hat{u}}{\hat{t}} + \frac{\hat{t}}{\hat{u}} - \frac{9}{4} \frac{\hat{u}^2 + \hat{t}^2}{\hat{s}^2} \right]$$

$$\frac{d\sigma}{d\cos\theta_*} (ug \rightarrow ug) = \frac{2}{9} \frac{\pi\alpha_s^2}{s} \left[-\frac{\hat{u}}{\hat{s}} - \frac{\hat{s}}{\hat{u}} + \frac{9}{4} \frac{\hat{u}^2 + \hat{s}^2}{\hat{t}^2} \right]$$

$$\frac{d\sigma}{d\cos\theta_*} (gg \rightarrow gg) = \frac{9}{4} \frac{\pi\alpha_s^2}{s} \left[3 - \frac{\hat{s}\hat{u}}{\hat{t}^2} - \frac{\hat{s}\hat{t}}{\hat{u}^2} - \frac{\hat{t}\hat{u}}{\hat{s}^2} \right]$$

with the other cases following using particle-antiparticle symmetry. Cross sections with identical particles in the final state should be integrated over $\cos\theta > 0$ only.

A comparison of the formula above to CDF data using the leading order formulae is shown in Figs p. 13. Figs p. 14 and 15 shows a careful modern version of this comparison by the CDF experiment, using QCD formulae that include the first higher-order corrections. The agreement between theory and experiment is quite remarkable. In particular, QCD theory tracks the experimental data as it falls by 8 orders of magnitude from a jet p_T of 50 to a jet p_T of 600 GeV.